Journal of Engineering Physics and Thermophysics, Vol. 76, No. 4, 2003

NUMERICAL ANALYSIS OF THE INFLUENCE OF THE ANGLE OF ATTACK ON A TURBULENT FLOW AROUND A THICK PROFILE WITH VORTEX CELLS AT HIGH REYNOLDS NUMBERS

S. A. Isaev, P. A. Baranov, N. A. Kudryavtsev, I. A. Pyshnyi, and A. G. Sudakov

UDC 532.517.4

A numerical investigation of the influence of the angle of attack on a turbulent flow around a thick profile with vortex cells at high Reynolds numbers has been carried out using the multiblock approach to solution of steady-state two-dimensional Reynolds equations closed by means of Menter's zonal model of shear-stress transfer.

Genesis and Objective of the Investigation. Continuing the series of recent works [1–6] devoted to numerical analysis of flow around a thick profile with built-in vortex cells, in the present work we refine and investigate in detail the influence of the angle of attack, changing in a wide range, on a turbulent flow around a thick profile with vortex cells at high Reynolds numbers. In this respect, our investigation develops the methods of control of flow around an "Ékip"-type aircraft of integral arrangement [7, 8].

As has been shown in [1–3], a flow around a two-dimensional model of the indicated apparatus representing a thick (of the order of 45% in fractions of the chord) profile separates, and the character of flow around this body with a bad aerodynamic shape does not change when passive vortex traps or vortex cells of elliptical shape are positioned on its back side. Intensification of the circulatory motion in the vortex cells by creating a momentum along their generatrices or as a result of suction from the central bodies positioned in them [4–6] substantially changes the structure of the flow to the extent that an unseparated regime of flow around the thick profile is established at a sufficient level of the controlling action.

The preliminary numerical calculations [4, 6] carried out with the use of the high-Reynolds version of the two-parameter dissipative model of turbulence made it possible for the most part to determine the qualitative regularities of flow around a thick profile and the behavior of its aerodynamic characteristics in a narrow range of angles of attack (from -10 to 10^{o}) at comparatively low Reynolds (Re) numbers (of the order of 10^4). In [6], the additional drag which is due to the expenditure of energy for creation of suction from the central bodies and maintenance of a near-unseparated regime of flow around a profile has been estimated.

In [5, 8], the application of Menter's low-Reynolds zonal mode of shear-stress transfer made it possible to refine and thoroughly analyze the influence of the Reynolds number on a turbulent flow around a thick profile and determine the threshold value of the Re number after the attainment of which the lift coefficient remains practically unchanged. This value of $\mathrm{Re} = 10^5$ is used in the present investigation devoted to estimating the influence of the angle of attack. It should be noted that in the present work, as in [5, 8], the velocity of suction from the central bodies is assumed to be constant (5% of the velocity of the incoming flow).

One more circumstance is of discussional interest. In a number of works [9–11] concerning the problem under consideration, including works carried out in the mid-1990s, analysis of flow around a wing profile (in a two-dimensional definition) with an isolated vortex trapped in a cavity was carried out using asymptotic models like the Batchelor model, which were oriented to modeling of circulation flows in cavities built into the contour of a body at limiting high Reynolds numbers. In [11], this situation with a trapped vortex was interpreted as a vortex cell, and the flow circulating in the cavity was intensified by rotating the circular cylinder positioned in it. It should be noted that only configurations with a single cavity, i.e., with a single trapped vortex, were considered in this case.

Academy of Civil Aviation, St. Petersburg, Russia; email: isaev@SI3612.spb.edu. Translated from Inzhenerno-Fizicheskii Zhurnal, Vol. 76, No. 4, pp. 115–124, July–August, 2003. Original article submitted August 14, 2002.

1062-0125/03/7604-0877$25.00

A weakness of this approach to modeling of flow around a profile (which, by the way, has little in common with a thick profile) is the assumption that the flow around the investigated body is unseparated and a single large-scale vortex exists within the vortex cell. This assumption seems to be unwarrantedly optimistic in light of the numerical investigations carried out in [1–6, 8], because it is practically impossible to prevent the formation of local separation zones in the case of flow around configurations close to real ones.

One of the objectives of the present investigation is also comparative analysis of profiles having a different thickness by their ability to create a lifting force at an angle of attack changing in a wide range, including the case where means for control of flow around thin profiles are used.

Methodology of Solution and Formulation of the Problem. As has already been described in detail [8], multiblock computational technologies have been developed for the purpose of forecasting the behavior of a separated flow around bodies with vortex cells. Of course, these developments do not claim to be pioneering, because it is very difficult to come up with ideas that were not tested earlier (in the 1970s–1980s). However, up till now not all of the progressive ideas have become implemented into computational practice. Among them is the conception of application of structurized block grids, which has being developed successively by us since the mid-1990s. It should be emphasized that the problems on a fluid flow in multiply connected regions formulated in this period generated the approach to their calculation on the basis of intersecting ○-type grids. Thereafter, the developed computational technology involving the superposition of grids of simple topology and different types made it possible not only to consider fairly complex configurations of bodies composed of a number of elements, but also to determine important, different-scale, structural features of the flow on specially introduced grids. Besides the solution of two-dimensional problems, the methodology has been extended to three-dimensional problems.

Initially (see, e.g., [2]), the choice of block computational grids was associated with the need for correct description of the configuration of a body with vortex cells built into it; polar grids with a constant pitch along the angular coordinate were used for this purpose. This approach was considered as wholly acceptable for a long time, the more so the multiblock grids (multistage with a different density of the near-wall points) made it possible to pass from the two-parameter dissipative Launder–Spalding model of turbulence to Menter's zonal model of shear-stress transfer [12]. The latter model has been tested in the case of stationary turbulent flows, in particular, in solving problems on the movement of a low-velocity air flow in rectangular [13] and extending [14] channels with a circular vortex cell on one of the walls, including the case where a rotating cylinder is located inside the cell. For these problems, physical experiments have been carried out on a special setup at the Institute of Mechanics of the Moscow State University. Menter's model has also been verified when applied to the solution of traditional test problems on a steady turbulent flow around a circular cylinder with a separating plane in the near wake [15] and an unsteady turbulent flow around a circular cylinder in a subcritical regime [16]. In the last cases, the calculated forecasts of the surface-pressure distributions (averaged over the period of variations of the transverse-force coefficient in a nonstationary regime) are comparable to the experimental data of Roshko [17] and Igarashi [18].

In recent years [8, 19], the multiblock approach was improved with the use of different-scale grids, including elliptical grids. This is explained in many respects by the desire to correctly describe the very fine features of the flow, in particular, in the neighborhood of rounded edges. It should be noted that in this case, improvement of the computational complex does not touch its core — the single-block solver. The latter was formed in the late 1980s early 1990s [20], and to date its characteristics remain practically unchanged [21]. In its conceptual content the solver represents an implicit finite-difference algorithm based on splitting by physical processes, which is a variety of the SIMPLE-like algorithms.

It is significant that the algorithm proposed differs in a number of positions from the traditional analogs [22] because it reflects the ideas of control of the computational process which are characteristic of the methods of calculation of compressible potential flows. This, first of all, refers to the designing of a discrete model for the increments of dependent variables and the application of schemes of approximation of different order for the implicit and explicit sides of linearized initial equations. It is suggested that the discretization of the implicit side is directly dependent on the computational stability of the computational algorithm. In this case, the use of coarse schemes makes it possible to most rapidly smooth out and decrease the level of the increments of the dependent variables. Therefore, in the methodology proposed, the upwind, one-sided differences of the first order of approximation are used for the convective terms, and in the diffuse terms the transport coefficient is increased by multiplying it into the scheme parameter OTL

(OTL > 1). The introduction of OTL also makes it possible to successfully smooth out the nonphysical oscillations of the parameters of a flow at high Reynolds numbers. As a matter of fact, this is the main original characteristic feature of the algorithm proposed.

The use of Leonard's quadratic upwind scheme in the explicit side of linearized equations of change in momentum has long been an approved method of decreasing the influence of the effects of numerical diffusion caused by errors in the approximation, first of all, of the convective terms of the equations. However, in the traditional SIMPLE-like algorithms [21, 22], for which the initial equations are usually written relative to the dependent variables themselves (but not relative to their increments), the use of Leonard's scheme leads to complications in the convergence of the computational process. In this algorithm the quadratic upwind scheme is used everywhere for solution of various multidimensional stationary and nonstationary problems at a fairly high (of the order of 0.5) relaxation coefficient.

In the case where a centered template is used, the known consistent SIMPLEC procedure of pressure correction [21, 22], in combination with the Rhie–Chow approach to interpretation of the relation between the fields of velocity and pressure, successfully correlates with the general approach to solution of the transport equations for increments of the Cartesian velocity components. Moreover, the use of the method of incomplete matrix factorization for solution of difference equations improves the convergence of the local iterations.

Some comments on calculation of the turbulence characteristics need to be made. As mentioned above, in recent years a change was made from the traditional two-parameter dissipative model of turbulence to the zonal low-Reynolds model of shear-stress transfer. However, in principle, the turbulence block in the solver has not been changed significantly, because two partial differential equations representing analogs of the generalized transport equation are solved for the characteristics of turbulence in both models. On the basis of these equations, the eddy-viscosity field is recalculated, which is then used for determining the coefficients of diffusion transfer. The discretization of the convective terms of the transport equations of the turbulence characteristics is performed by the UMIST scheme, which is a variety of the TVD scheme [16]. The only difference concerns the calculation of the near-wall terms in the equations of the low-Reynolds model of turbulence, which require the estimation of the distance from the wall.

The computational multiblock algorithm developed [8] is based on the procedure of global iterations, which has been constructed for solving transport equations by the finite-volume method on structurized intersecting H- and ○-type grids. On the whole, the oblique grids are subdivided into computational and connected meshes. In meshes of the first type, the flow equations closed by the differential equations of the turbulence characteristics are solved. In the connected meshes positioned in the near-boundary zones of the computational subregions and in the zones of intersecting of grids, the parameters are determined by means of linear interpolation [19, 23].

The iteration algorithm considered is characterized by the following features: (a) determination of the preliminary Cartesian velocity components for the frozen fields of eddy viscosity and pressure at the predictor step with subsequent correction of the pressure on the basis of the solution of the continuity equation with corrections for the velocity field and (b) calculation of the fields of turbulence characteristics and eddy viscosity for the frozen velocity fields. A computational process is constructed such that to one predictor step correspond several local iteration steps in the block of pressure correction. The global iterations are completed when the fields of dependent variables converge with a given acceptable accuracy [16].

In such a way, a computational means for forecasting the characteristics of a turbulent flow around curvilinear, composite objects is formed.

In the present work, a refined numerical investigation, (as compared to [3–6]) of turbulent flow around a thick profile with four vortex cells — a model of the "Ekip" apparatus — is carried out for the configuration with slightly rounded sharp-pointed edges (Fig. 1). In this case, the length of the chord of the profile l is taken as the characteristic dimension, and so the other linear dimensions are expressed in fractions of its length. The angle of attack varies from –30 to 25^{o}.

The contour of the aerodynamic body is composed of an upper circular arc of radius 0.577 and two lower circular arcs of radius 0.175, connected by a segment with a coordinate $y = -0.0866$. The radius of the rounding of the leading and trailing sharp-pointed edges is taken to be 0.05.

The arc coordinate of the center of the window of the first cell is equal to –0.685. The length of the window is 0.0834. The elliptical cell (Fig. 1a) with a longitudinal semiaxis $a_x = 0.0584$ and a transverse semiaxis $a_y = 0.5a_x$ is built deeper into the contour of the thick profile a distance $y_0 = 0.7a_y$. The radius of the rounding of the sharp-

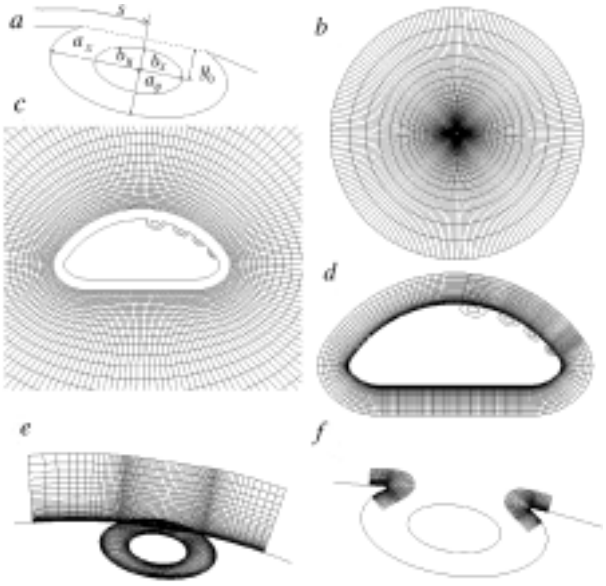

Fig. 1. Scheme of a thick profile in the body-axis system, elliptical shape of a vortex cell with rounded sharp-pointed edges, built into the thick profile (a), configuration of the computational region (b), and fragments of the grids positioned at a large distance from the profile (c), near it (d), inside and over the vortex cell (e), and near the rounded edges (f).

pointed edge of the cell is 0.001. Bodies of elliptical shape with a longitudinal semiaxis $0.5a_x$ and a transverse semiaxis $0.25a_x$ are positioned at the centers of the cells.

The other three cells are topologically identical to the first cell. Their arc coordinates are –0.861, 0.992, and 1.107, the dimensions of the windows are 0.0696, 0.0556, and 0.0417, the longitudinal semiaxes are 0.0487, 0.0389, and 0.0292, and the radii of the roundings of the sharp-pointed edges are 0.00084, 0.00067, and 0.00051, respectively.

The parameters of an undisturbed flow are prescribed at the inlet of the outer boundary of the computational region. The characteristics of turbulence are formulated just as in [3–6, 15] and correspond to the conditions of physical experiments performed in wind tunnels. Thus, the turbulence energy at the inlet boundary k_∞ corresponds to the degree of turbulence of the incoming flow (Tu_∞ = 1.5%) and the scale of turbulence L_∞ is of the order of the characteristic linear dimension of the problem.

The soft boundary conditions (the conditions of continuation of solution) are set at the outlet of the outer boundary, and the adhesion conditions are set on the surface of the body, including the contours of the vortex cells.

The velocity of distributed uniform suction on the surfaces of the central bodies in the vortex cells $V_{\mathrm{n}i}$ is expressed in fractions of the velocity of the incoming flow U_∞ (i is the number of a vortex cell, the index i is omitted when the velocities of suction in the vortex cells are equal). In this case, $V_{\mathrm{n}i}$ = 0.05. The total coefficient of flow rate c_q of the air exhausted via the cells is determined. The considered model of intensification of a vortex flow in a cell reflects, to a certain extent, the process of intake of air through a porous insert on the basis of its ejection with the help of a propulsion system.

The velocity of the incoming flow U_∞ is also taken as the dimensionless scale.

In the case of suction from the surface of the central bodies in the vortex cells, the additional drag is determined, as in [6], in terms of the power necessary to maintain the rate of the fluid flow through the central bodies by analogy with the approach used in [15] for estimating the additional drag of a cylinder with rotating small-diameter cylinders built into its contour. For the profile with four cells

$$C_{x\mathrm{add}} = 4N_q \Big/ \left(\frac{1}{2}\,\rho U_\infty^3\, l\right) = 2\,\Sigma p_{\mathrm{cp}i} c_{qi}\,.$$

As a result, we determine the dependence $C_x(V_{\mathrm{n}})$, where $C_x = C_{x\mathrm{cal}} + C_{x\mathrm{add}}$ is the drag coefficient of the cylinder with vortex cells, corrected for the expenditure of energy.

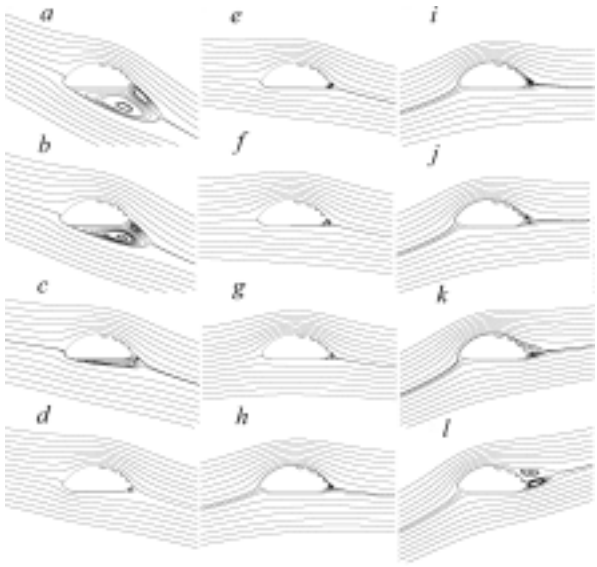

Fig. 2. Pattern of flow around a profile with active vortex cells (the velocity of suction from the central bodies is equal to 0.05) at Re = 10^5 and angles of attack α equal to -30^o (a), -25^o (b), -17.5^o (c), -16.5^o (d), -10^o (e), -5^o (f), 0^o (g), 5^o (h), 10^o (i), 15^o (j), 20^o (k), and 25^o (l).

Computational Grid and Scheme Parameters. The thick profile is surrounded by a three-stage computational grid (Fig. 1b–d). The 0.1-thick ring layer adjacent to the contour contains 30 meshes in the transverse direction. Forty meshes are positioned between the nose of the profile and the first vortex cell, 10 meshes are positioned on the vortex cells, 10 meshes are positioned between them, and 120 meshes are positioned between the last vortex cell and the leading edge of the profile. The dimension of the grid pitch near the surface is 0.0001. The second and third ring layers of thickness 3 and 35 contain 30 and 20 meshes in the radial direction and 160 meshes over the peripheral coordinate. The dimension of the longitudinal pitch near the sharp-pointed edge is 0.01.

Each vortex cell (Fig. 1e) is covered by an individual external grid adjacent to its window. The vertical dimensions of all the subregions are 0.05, the number of meshes along the normal to the wall is 30, and the dimension of the near-wall pitch is 0.0001. The dimensions of the regions in the direction of flow before and behind the vortex cells are 0.0607, 0.0506, 0.0404, and 0.0304, and the number of meshes found in these spacings is 20 and 15. The meshes are arranged with a bunching in the neighborhood of the edges. The near-edge pitch is taken to be 0.001.

Inside each vortex cell, a cylindrical grid is constructed with a bunching of points to the walls of the cell and the central body (the near-wall pitch is 0.0001) and in the regions of the cell adjacent to the sharp-pointed edges (the minimum pitch is 0.001). Forty meshes are positioned in the radial direction. The region of a vortex cell is divided along the peripheral coordinate into two subregions bearing up against the lower and upper semiarcs, which are divided into 40 and 20 meshes, respectively.

The neighborhood of the leading and trailing edges (Fig. 1f) of the vortex cells is covered by curvilinear fine grids. The grids are divided in the longitudinal direction into three regions: from the edge of the cell outward (15 meshes), on the rounding (8 meshes), and from the edge of the cell inward (15 meshes). Fifteen meshes are positioned with a pitch of 0.0001 along the normal to the surface.

The lower relaxation with coefficients for the velocity (0.5), pressure (0.8), characteristics of turbulence (0.5), and eddy viscosity (0.35) is introduced at each iteration step for stabilization of the computational process. The value of OTL is taken to be 2.5 in the solution of the equations of change in momentum and 1.5 in the turbulence block.

Analysis of Results. Some of the results obtained are presented in Figs. 2–6.

The evolution of the patterns of flow around the thick profile, presented in Fig. 2, demonstrates the transformation of the large-scale vortex structures with increase in the angle of attack from -30 to 25^o. Several typical situations can be separated.

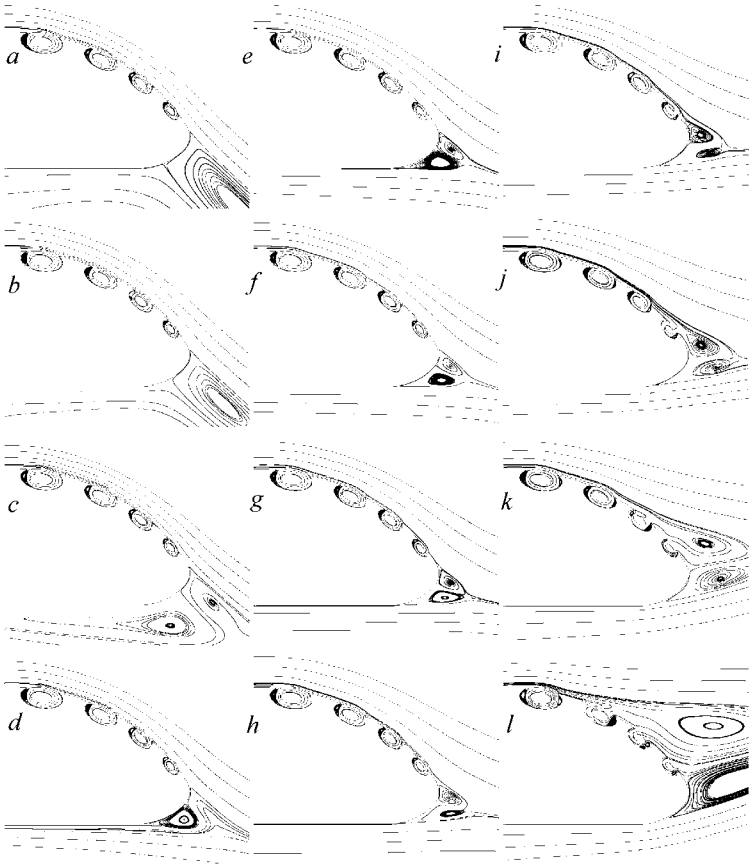

Fig. 3. Pattern of flow around the tail part of the profile. Notation is the same as in Fig. 2.

A zone of circulation flow, consisting of a pair of vortices, is formed under the bottom of the profile when α changes from -30 to -17.5^{o}. The flow separates from the profile in the neighborhood of the leading and trailing extremities at the sites of rounding of the sharp-pointed edges. The stagnation point of the flow (see Fig. 5) is positioned on the upper generatrix of the contour around which air flows. The flow around the convex part of the profile is unseparated.

The pattern of the flow under the profile bottom changes abruptly when α increases from -17.5 to -16.5^{o}; in this case, the separation point displaces suddenly from the nose extremity of the profile to the stern. Hereinafter, until the angle of attack is equal to 10^{o}, the flow around the thick profile is practically unseparated, not counting the small zone of circulation flow in the stern part which is formed because of the nonperfection of the chosen aerodynamic shape of the profile. It is interesting to note that, in this case, the leading stagnation point moves smoothly from the upper generatrix of the contour (the part of the circle) to the bottom of the profile (the linear segment).

And, finally, a separation zone begins to form in the stern part of the profile in the neighborhood of the upper generatrix when the angle of attack changes from 15 to 25^{o}. The reason for its appearance is the deterioration of the normal operation of the vortex cells at large α. As indicated above, the chosen velocity of suction in the vortex cells is quite sufficient to provide an unseparated regime of flow around a thick profile only at zero angle of attack. It should be noted that even in the preliminary investigations carried out at a moderate Reynolds number ($Re = 10^{4}$) it has been established that the back vortex cells cannot always cope with the separation of the flow from the curvilinear wall. Therefore, of interest is a detailed analysis of the pattern of flow in the tail part of a thick profile, presented in Fig. 3.

The point of separation of the flow on the upper generatrix of the contour around which air flows remains practically unchanged in the wide range of angles of attack from -30 to 5^{o}. At the same time, at the bottom, separation occurs first in the front part of the profile and then, beginning with $\alpha = -16.5^{o}$, moves to the stern part. At an

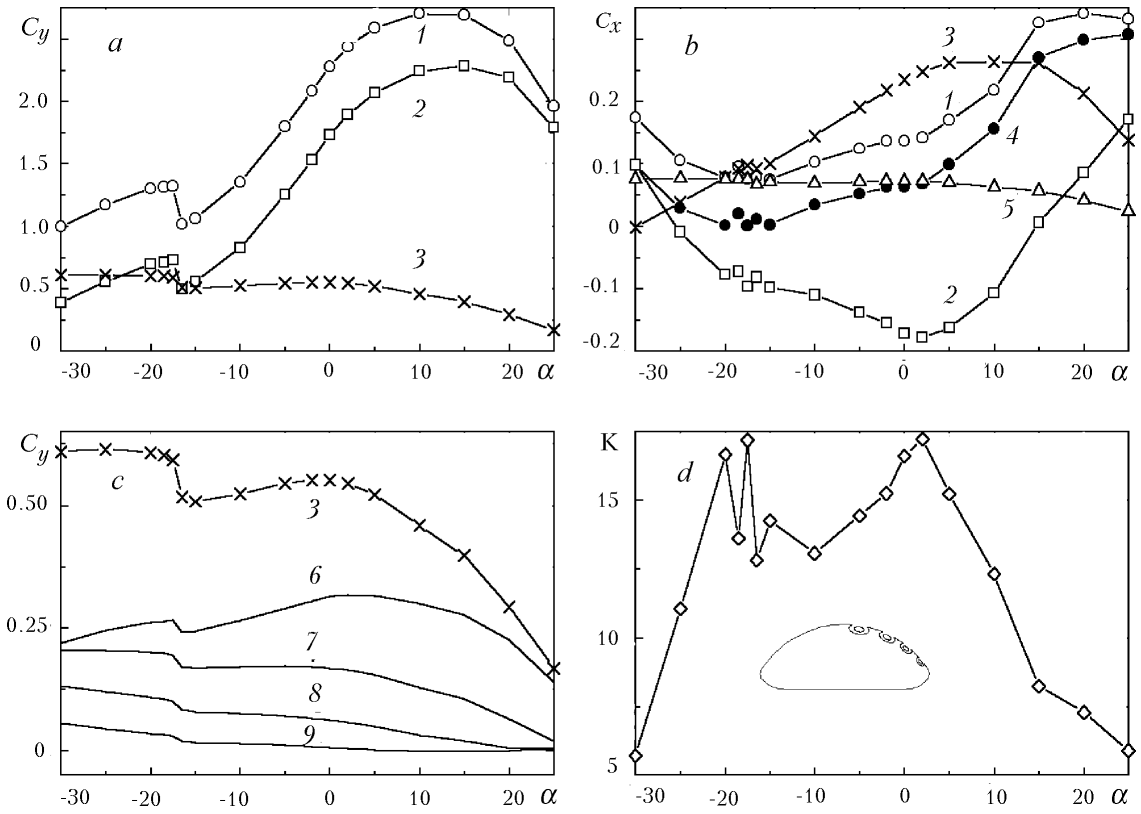

Fig. 4. Dependence of the force integral characteristics of the thick profile with vortex cells on the angle of attack α: a) lift coefficient, b) drag, c) lift coefficient of the set of vortex cells and of each individual vortex cell, and d) lift-to-drag ratio [1) for the profile with vortex cells (with regard for the expenditure of energy), 2) for the profile without vortex cells; 3) for the set of vortex cells, 4) forecasted values of the drag coefficient, 5) coefficient of additional drag caused by the expenditure of energy, and 6, 7, 8, 9) for the first, second, third, and fourth vortex cells, respectively].

angle of attack equal to 10^o the separation point moves upstream and approaches the back vortex cell. An analysis of the vortex structures, presented in Fig. 3j–l, shows that the vortex cells get out of order successively, beginning with the back cell (which is the fourth in succession), when the angle of attack increases. Thus, the given velocity of suction from the surface of the central bodies, equal to 0.05, is insufficient to provide an unseparated regime of flow around the profile. As a result, at $\alpha = 25^o$, only one (the first) vortex cell of the four cells functions in the system of control of flow around the thick profile.

The failure of the vortex cells influences first of all the lifting force of the thick profile (Fig. 4a), gradually decreasing C_y when α increases from 15 to 25^o. In principle, the above-indicated movement of the separation point upstream from the back extremity of the upper contour (Fig. 3i) is evidence of the inability of the system of control of the flow to cope with the separation of the flow in the stern part; in this case, $C_y(\alpha)$ achieves a maximum value close to 2.75. At all the other angles of attack, C_y increases monotonically, except for the jump-like decrease at $\alpha \approx -17^o$, which corresponds to a sudden displacement of the separation point at the bottom of the profile.

It is interesting to note that there are opposite tendencies in the behavior of $C_y(\alpha)$ for the profile itself and a set of vortex cells. The force load (curve 2) measured for the contour (without regard for the vortex cells) practically copies $C_y(\alpha)$ for the object considered.

As has been shown earlier [5], vortex cells built into the contour of a body around which air flows are generators of circulation (this phenomenon was interpreted as a supercirculation effect) which give rise to a significant lifting force. This means that the lifting force of an unseparated flow around a thick profile with vortex cells is much

greater (by 20–30%) than the lifting force of an unseparated flow around a smooth contour. The efficiency of vortex cells to reproduce the lifting force decreases with increase in the angle of attack, even though not very significantly. It is interesting to note that the transformation of the pattern of flow around the profile at $\alpha \approx -17^o$ influences the circulatory motion of air inside the vortex cells, causing a small jump-like change in the force characteristics (curve 3 in Fig. 4a).

As follows from Fig. 4b, the calculated drag coefficient $C_{x\text{cal}}$ (curve 4) determined by the surface distributions of the static pressure has a minimum at a negative angle of attack in the range from –20 to -15^o, in which the pattern of a separated flow transforms. It should be emphasized that the value of this minimum is very close to zero. A subsequent increase in α to 0^o is accompanied by a small increase in $C_{x\text{cal}}$ — approximately to 0.06. At $\alpha > 0^o$ the drag begins to increase rapidly; however after $\alpha = 15^o$ the rate of increase sharply decreases and $C_{x\text{cal}}$ becomes minimum at $\alpha = 25^o$.

The described behavior of $C_{x\text{cal}}(\alpha)$ can be explained on the basis of analysis of its components: the drag of the smooth profile itself (without cells, curve 2) and the total drag of the vortex cells (curve 3). It is significant that in the fairly wide range of angles of attack from –20 to -15^o, C_x of the smooth profile is negative, i.e., a driving force acts on the profile around which air flows in an unseparated regime. It reaches its largest value, equal to –0.17, at $\alpha = 2^o$. Of course, the driving force is completely compensated by the drag of the vortex cells. The total drag of the vortex cells C_x increases from 0 to approximately 0.25 when the angle of attack changes from -30 to 5^o. After the small "shell," at $\alpha > 15^o$ C_x begins to decrease sharply. Thus, the traditional increase in the drag of the profile with increase in α is caused by the increase in the contribution of the smooth contour of the body to C_x at large angles of attack.

An estimation of the additional drag caused by the expenditure of energy for suction of air from the surface of the central bodies in the vortex cells has shown that its dependence on the angle of attack is qualitatively similar to $C_y(\alpha)$ of the vortex cells. Only the jump-like change in $C_{x\text{add}}$ as a result of the transformation of the separated flow around the thick profile is even less marked. In a wide range of α (approximately to 10^o), the additional drag of the profile changes insignificantly and its level is of the same order as the calculated drag of the thick profile with vortex cells at $\alpha = 0^o$. At larger angles of attack the contribution of the additional drag to the total drag of the body decreases even though the total drag of the profile is high at the indicated angles of attack.

Thus, in the case where the angle of attack increases, the total drag resistance of the thick profile with active vortex cells (curve 1) is very close in behavior to the drag calculated by the distribution of the surface pressure (curve 4). The minimum value of the drag coefficient of the body was found to be equal to 0.08. It should be noted that the total drag determined with regard for the expenditure of energy has a local maximum at $\alpha = 20^o$, i.e., the thick profile with a system of control of flow around it differs from the traditional profiles.

The behavior of C_y of the vortex cells on change in α is shown in detail in Fig. 4c, taking into account the contribution of each cell. Whereas the first vortex cell generates a lifting force progressing with increase in the angle of attack, the contribution of the other cells decreases monotonically. As mentioned above, the last three cells fail at large α, with the result that the lifting force practically disappears. It is interesting that at $\alpha = 0^o$ the total lift coefficient has a local maximum ($C_y = 0.53$) that does not coincide with the local maxima of the individual vortex cells. And, of course, the contribution of the first cell to the formation of the total lifting force is predominant, especially at positive angles of attack.

An estimation of the lift-to-drag ratio of the thick profile with vortex cells has revealed two local maxima, equal to 17.5. One of them is multivalued because it falls in the range of negative angles of attack, in which a separated flow is transformed. The second maximum corresponds to the neighborhood of small positive angles of attack (2^o). The local minima of the lift-to-drag ratio, having a value of the order of 12.5, are realized at negative angles of attack lying in the range from -17.5 to -10^o. It should be noted that a fairly large lift-to-drag ratio of the thick profile in the range from 12.5 to 17.5 is attained in the wide range of angles of attack from -23 to 10^o.

The level of the lift coefficient $C_y > 1$ attained for the thick profile in the considered range of angles of attack from -30 to 25^o should be considered as the most important of the results presented in Fig. 4. Since this result seems somewhat unexpected, especially in the region of negative α, the evolution of the profiles of the surface pressure with increase in the angle of attack is analyzed in Fig. 5.

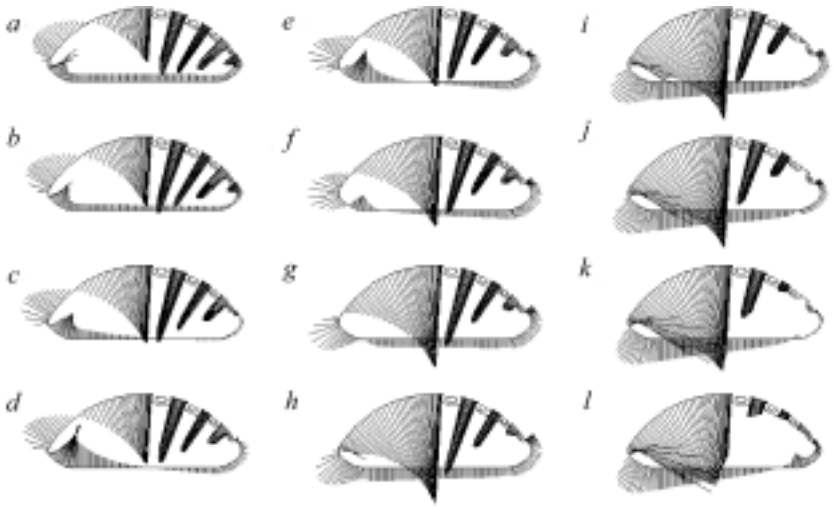

Fig. 5. Diagrams of the surface pressure for the profile with active vortex cells at different angles of attack α (without regard for the walls of the vortex cells, around which air flows). Notation is the same as in Fig. 2.

Actually, as follows from Fig. 1a–c, at larger negative angles of attack a developed separation zone is formed under the bottom of the thick profile. Consequently, a zone of decreased pressure is formed at the bottom. Moreover, the flow runs on the profile from above and so a zone of increased pressure is formed in the front part of the upper generatrix of the contour of the body. The indicated surface loads must generate a negative lifting force. At the same time, it follows from Fig. 4 that the lift coefficient of the profile itself without vortex cells comprises 0.4–0.6 in this range of α. Such positive values of C_y are realized due to the predominant contribution of the zone of very high negative pressure on the back of the upper generatrix of the contour to the lifting force. The force arising in this case not only compensates the above-indicated negative lifting force, but also forms C_y on the profile, which is of the same order as the total lift in the vortex cells.

It is interesting to analyze the reasons for the jump-like change in C_y of the profile without vortex cells in the case shown in Fig. 5c, d. The movement of the separation point from the front part of the contour to the back part and the actual attachment of the flow to the bottom increase the discharge in the nose part of the bottom and simultaneously increase the pressure in the stern part. But the main reason is a significant decrease in the level of discharge on the back surface of the contour.

As mentioned above, as the angle of attack becomes larger than -16.5°, the zone of increased pressure corresponding to the front stagnation point moves from the upper part of the contour to the bottom, aiding in increasing C_y. In this case, the zone of decreased pressure in the front part of the bottom disappears and is replaced by a wide region of increased pressure which extends throughout the length of the bottom (which also stimulates C_y to increase). By the way, the indicated region represents a zone with an approximately constant pressure gradient. True, at negative α the flow in the neighborhood of the bottom decelerates under the action of the positive pressure gradient, and at positive α the flow under the profile, on the contrary, accelerates in the zone with a negative pressure gradient.

The upper part of the contour becomes a powerful generator of the lifting force when the angle of attack increases. The progressing discharge in the front part of the contour decelerates slightly at large angles of attack.

At large α, the flow in the back part of the profile re-forms, with the result that the discharge decreases. It is apparent that the failure of vortex cells is accompanied by an increase in the pressure in the zones of their disposition and, consequently, a decrease in the lifting force of the profile.

Figure 6 combines the results of the methodical experiments for thick profiles close in geometry with vortex cells and the data of the comparative analysis of flows around thick and thin profiles, including the case where there is a system of control of their circulation.

The aim of the methodical experiment is to estimate the degree of adequacy of the numerical forecasts of the characteristics of a flow around a thick profile with vortex cells. This aim is attained by comparing the data on C_y(Re) for the profile with cells and for the profile itself (without cells), taken from [5] and [8]. As follows from Fig. 6a, at

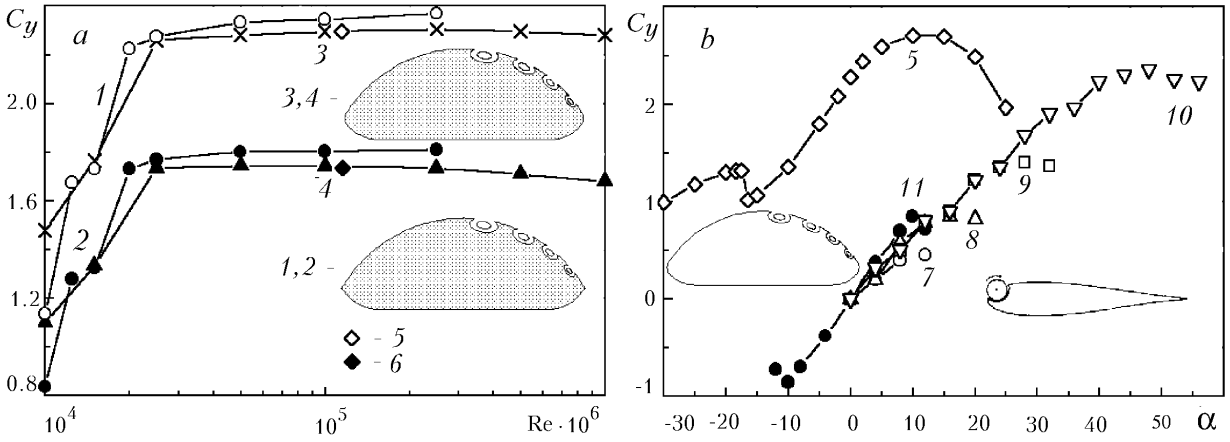

Fig. 6. Comparative analysis of C_y for thick profiles close in geometry with vortex cells at different values of Re (a) and for thick and thin profiles, including the case where a rotating cylinder is built into their nose part, at varying α and a fixed Re (b) equal to 10^5 for the thick profile and $4.62 \cdot 10^4$ for the thin profile. The numbered curves correspond to the thick profiles close in geometry with vortex cells (1, 3, 5), the profiles without vortex cells (2, 4, 6), the Zhukovskii profile with a built-in cylinder rotating with a velocity V_t = 0 (7), 1 (8), 2 (9), and 4 (10), and the Zhukovskii profile itself (11).

Re = 10^5 the results of the present work are in good agreement with the data obtained at the same level of the control action. This can be considered to a certain extent as evidence of their adequacy and the acceptability of the computational complex for forecasting the characteristics of thick profiles with active vortex cells.

The present numerical investigation would undoubtedly be incomplete if it did not include a comparison of data on the characteristics of thick and thin profiles. For this purpose, we used the experimental data of [24] for the Zhukovskii thin profile (of thickness 0.14) in the standard variant and a profile equipped with a system of control of flow in the form of a rotating cylinder positioned in the front part of the profile. The Reynolds number was selected to be $4.62 \cdot 10^4$. By varying the rotational velocity V_t measured on the surface of the cylinder, the effect of adhesion of the flow to the upper generatrix of the profile positioned at an angle of attack ($\alpha = 20^o$ in [24]) is attained (at high V_t of the order of 4).

A comparative analysis of the results presented in Fig. 6b shows that a thick profile with active vortex cells has the indubitable advantage as a generator of the lifting force. It is significant that for symmetric thin smooth profiles, C_y is limited by the value of the order of unity. Moreover, at negative α $C_y < 0$, which is not always useful in applications. Even though a rotating cylinder positioned in the nose of a thin profile significantly increases the lift coefficient, the profile must be set at large angles of attack in order that the lifting force be realized. It has been established in experiments [24] that the cylinder must rotate with a high velocity (of the order of 4) to provide an unseparated regime of flow around the profile, which calls into question the economical expediency of this method of control.

Thus, at zero angles of attack the aerodynamic characteristics of a thick profile with active vortex cells differ greatly from the analogous characteristics of the traditional profiles, which makes it possible to significantly widen the field of their application.

The authors are grateful to Yu. M. Lipnitskii for useful discussion of the problem.

This work was carried out with financial support from the Russian Foundation for Basic Research (projects 02-01-00670, 02-02-81035, and 02-01-01160).

NOTATION

x, y, Cartesian coordinates in the body-axis system, fractions of the chord; α, angle of attack, deg; *s*, coordinate measured along the contour of the cylinder, fractions of the chord; ρ, density of fluid, kg/m^3; U_∞, velocity of an

undisturbed flow, m/sec; l, length of the chord, m; μ, dynamic coefficient of viscosity, kg/(m·sec); k, energy of turbulent pulsations, fractions of U_∞^2; ω, specific rate of turbulence dissipation, dimensionless; L, scale of turbulence, fractions of l; Tu, degree of turbulence of the flow, fractions of U_∞; $\mathrm{Re} = \rho U l/\mu$, Reynolds number; a_x, a_y, dimensions of the semiaxes of the elliptical vortex cell, fractions of l; y_0, coordinates of the central cell, fractions of l; b_x, b_y, dimensions of the semiaxes of the elliptical central body, fractions of l; V_n, velocity of suction from the surface of the central body, fractions of U_∞; V_t, rotational velocity on the surface of the central body, fractions of U_∞; C_p, pressure coefficient; $C_{x\mathrm{cal}}$, drag coefficient; $C_{x\mathrm{add}}$, coefficient of additional drag caused by the expenditure of energy for the maintenance of suction from the surface of the central bodies; C_x, drag coefficient corrected with regard for the expenditure of energy; C_y, lift coefficient; $K = C_y/C_x$, lift-to-drag ratio; N_q, power necessary to maintain suction from the surface of the central body in the cell, kg·m/sec^3; c_q, flow rate through the surface of the central body, fractions of $U_\infty l$; p_m, mean static pressure (related to the double kinetic head ρU_∞^2) on the surface of the central body in the cell. Subscripts: i, number of a vortex cell; ∞, parameters of the incoming flow; n, normal; t, tangential; cal, calculated; add, additional; m, mean.

REFERENCES

1. S. A. Isaev, Yu. S. Prigorodov, and A. G. Sudakov, *Inzh.-Fiz. Zh.*, **71**, No. 6, 1116–1120 (1998).
2. P. A. Baranov, S. A. Isaev, Yu. S. Prigorodov, et al., *Izv. Vyssh. Uchebn. Zaved., Aviats. Tekh.*, No. 3, 30–35 (1999).
3. P. A. Baranov, S. A. Isaev, Yu. S. Prigorodov et al., *Inzh.-Fiz. Zh.*, *72*, No. 3, 572–575 (1999).
4. P. A. Baranov, S. A. Isaev, Yu. S. Prigorodov et al., *Inzh.-Fiz. Zh.*, **73**, No. 4, 719–727 (2000).
5. S. A. Isaev, A. G. Sudakov, P. A. Baranov, et al., *Dokl. Ross Akad. Nauk*, **377**, No. 2, 1–3 (2001).
6. S. A. Isaev, Yu. S. Prigorodov, and A. G. Sudakov, *Inzh.-Fiz. Zh.*, **75**, No. 3, 47–50 (2002).
7. L. N. Shchukin, A. P. Shibanov, I. L. Shchukin, et al., *Method of Control of the Boundary Layer on the Aerodynamic Surface of a Flying Vehicle*: RF Patent 2015941, Byull. No. 13, 71 (1991).
8. A. V. Ermishin and S. A. Isaev (eds.), *Control of Flow Past Bodies with Vortex Cells as Applied to Flying Vehicles of Integral Arrangement (numerical and physical modeling)* [in Russian], Moscow–St. Petersburg (2001).
9. A. V. Bunyakin, S. I. Chernishenko, and G. Yu. Stepanov, *J. Fluid Mech.*, **323**, 367–376 (1996).
10. A. V. Bunyakin, S. I. Chernishenko, and G. Yu. Stepanov, *J. Fluid Mech.*, **358**, 283–297 (1998).
11. A. V. Bunyakin, *Izv. Ross. Akad. Nauk, Mekh. Zhidk. Gaza*, No. 4, 87–92 (2001).
12. F. R. Menter, *AIAA J.*, **32**, No. 8, 1598–1605 (1994).
13. S. A. Isaev, S. V. Guvernyuk, M. A. Zubin, et al., *Inzh.-Fiz. Zh.*, **73**, No. 2, 220–227 (2000).
14. S. A. Isaev, P. A. Baranov, S. V. Guvernyuk, et al., *Inzh.-Fiz. Zh.*, **75**, No. 2, 3–8 (2002).
15. S. A. Isaev, Yu. S. Prigorodov, and A. G. Sudakov, *Izv. Ross. Akad. Nauk, Mekh. Zhidk. Gaza*, No. 4, 88–96 (2000).
16. S. A. Isaev, V. L. Zhdanov, P. A. Baranov, et al., *Numerical Modeling of Laminar and Turbulent Flows Past a Circular Cylinder with Inner Channels and Windows in the Contour* [in Russian], Preprint No. 5 of the A. V. Luikov Heat and Mass Transfer Institute, Minsk (2002).
17. A. Roshko, *On the Drag and Shedding Frequency of Two-Dimensional Bluff Bodies*, NACA Tech. Note, No. 3169 (1954).
18. T. Igarashi, *Bull. JSME*, **21**, No. 154, 654–664 (1978).
19. S. A. Isaev, in: *Proc. Int. Conf. on Methods of Aerophysical Research*, Pt. 1, Novosibirsk (2002), pp. 102–107.
20. I. A. Belov, S. A. Isaev, and V. A. Korobkov, *Problems and Methods of Calculation of Separated Flows of an Incompressible Fluid* [in Russian], Leningrad (1989), pp. 618–631.
21. S. A. Isaev, N. A. Kudryavtsev, and A. G. Sudakov, *Inzh.-Fiz. Zh.*, **71**, No. 4, 618–631 (1998).
22. J. H. Ferziger and M. Peric, *Computational Methods for Fluid Dynamics*, Springer-Verlag, Berlin (1999).
23. S. A. Isaev, A. I. Leont'ev, P. A. Baranov, et al., *Inzh.-Fiz. Zh.*, **74**, No. 2, 62–67 (2001).
24. V. J. Modi, M. S. U. K. Fernando, and T. Yokomizo, *AIAA J.*, **29**, No. 9, 1400–1406 (1991).